

# Linear/Nonlinear Dynamic Analysis and Prediction of Failure Mechanism of Irgandi Bridge

Gökhan Barış Sakcalı<sup>1\*</sup>, Alper Gönül<sup>2,3</sup>, Muhammed Bilal Bağbancı<sup>3</sup>, İsa Yüksel<sup>1</sup>

<sup>1</sup> Department of Civil Engineering, Faculty of Engineering and Natural Sciences, Bursa Technical University, Yıldırım Bayezid Campus, 16330, Bursa, Turkey

<sup>2</sup> Department of Architecture, Faculty of Architecture and Design, Bursa Technical University, Yıldırım Bayezid Campus, 16330, Bursa, Turkey

<sup>3</sup> Department of Architecture, Faculty of Architecture, Bursa Uludağ University, Görükle Campus, 16285, Bursa, Turkey

\* Corresponding author, e-mail: [gokhan.sakcali@btu.edu.tr](mailto:gokhan.sakcali@btu.edu.tr)

Received: 20 April 2022, Accepted: 28 August 2022, Published online: 08 September 2022

## Abstract

The goal of this study is to investigate the behavior and failure mechanism of historical Irgandi Bridge located in Bursa City under earthquake loads by using linear and nonlinear dynamic analysis. Dynamic characteristics of the bridge is investigated by using in-situ Operational Modal Analysis (OMA) tests. The finite element model is updated according to the OMA tests. Three different artificial earthquake records from weak to very strong are applied to the model for understanding the damage zones and the failure mechanism of the historical bridge. The results show that the bridge does not reach the failure mechanism under weak earthquakes for nonlinear dynamic analysis. However, under strong earthquake even if damage zones are occurred and the stiffness of the bridge is decreased, there is no failure mechanism observed according to the nonlinear dynamic analyses. Under very strong earthquake loads the bridge reaches the failure mechanism according to the nonlinear dynamic analysis. As the earthquake level increases, the difference between linear and nonlinear dynamic analysis results increases due to structural damages. In addition, considering the soil-structure interactions, it is concluded that the dynamic characteristics could be reflected more accurately.

## Keywords

finite element method, historic masonry bridges, linear dynamic analysis, nonlinear dynamic analysis, operational modal analysis

## 1 Introduction

Historical structures allow people to understand the development of past civilizations and the sites in which they lived and supply an apparent connection to the past. Moreover, they supply a visible connection to the past and may represent a significant era or a milestone in the history or particular style of architecture. For all these reasons, the preservation of historical structures with cultural heritage value is a prominent concern in advanced societies. It is necessary to determine their structural behaviors, and accordingly develop suggestions for strengthening and restoration to preserve the historical structures.

The notion of conservation is also on the agenda lately in Turkey, which hosts ancient ruins and historical structures from the Byzantine, Ottoman and Seljuk periods. Nineteen UNESCO world heritage sites belonging to different periods are located in Turkey historical bridges which were built due to the geographical location of Turkey

constitute an important part of the heritage. 80 bridges from the Roman period, 10 from the Byzantine period, 133 from the Seljuk period and 1059 from the Ottoman period are known to have been built in Turkey [1].

Historical Bridges have a vulnerable structure that can be easily damaged due to natural risks, manmade effects and deterioration caused by use [2]. For this reason, in order to conserve historical bridges, it is necessary to calculate bearing capacities, assess the response to the natural risks (such as earthquake, flooding) and take safety precautions.

Although the assessment of bearing capacity of historic bridges is traditionally based on simple observations supported by non-destructive methods. Non-destructive methods are generally used to determine the mechanical properties of materials in order not to damage historical structures [3–4]. There are also experimental or quasi-experimental evaluations based on destructive methods of

samples taken from structures and site tests in recent years. There are many studies that evaluate the structural behavior of historical structures, either numerically, experimentally, or updating of numerical models according to experimental tests. Dynamic characteristics of structures can be obtained more realistically from numerical models calibrated by experimental tests [5].

Linear or nonlinear dynamic analysis are performed to establish more realistic seismic behavior of the bridges by creating numerical models [6–10]. In order to examine the earthquake performance of the bridges, dynamic behavior is determined by using different calibration methods in many studies and numerical models are calibrated according to this behavior [11–14]. The seismic performance of the updated models is investigated. In some studies, material tests are carried out to update the numerical model and then the earthquake performance of the structure is determined [15].

It is of great importance to evaluate the structural performance of the Irgandi Bridge, one of the few bridges in the world with shops on it, so that it could be conserved and passed on to future generations. In this regard, restoration and reconstruction projects of the Irgandi Bridge were prepared and implemented under the leadership of Eyüpgiller et al. [16]. In addition, linear dynamic analysis of the idealized model was created to determine the seismic performance of the Irgandi Bridge by Sakcali et al. [17]. In this study, the finite element model of the Irgandi Bridge is created considering soil-structure interaction and the finite element model is updated by determining its dynamic behavior by using OMA (Operational Modal Analysis) [18] method. The linear and nonlinear dynamic analysis of the updated finite element model is performed under three different levels of artificial earthquake recording. As a result, the differences between linear and nonlinear dynamic analysis according to different earthquake levels are compared and the damage zone and potential failure mechanism are established as outcome of nonlinear dynamic analysis.

## 2 Material and method

### 2.1 Irgandi Bridge and finite element method

The Irgandi Bridge, spans over the Gökdere River in the city of Bursa in Turkey, was built as stone masonry in 1442 during the early period of Ottoman Empire. Irgandi Bridge is one of the few bridges in the world with shops on it (The other bridges with shops are Ponte Vecchio Bridge in Florence in Italy, Ponte di Rialto Bridge in Venice in

Italy, Osam Bridge in Lovech in Bulgaria). Until the 1855 Bursa Earthquake, there was a shopping precinct on the Irgandi Bridge, which was made of stone masonry and covered with a gable roof (Fig. 1(a)). The masonry precinct, which was probably seriously damaged in the 1855 earthquake, was completely removed and replaced with an open bazaar consisting of wooden shops on both two sides [19] (Fig. 1(b)) [20, 21].

The bridge and the shops on it were destroyed during the Turkish War of Independence in 1922. Without the shops on it, only the bridge structure was rebuilt using massive concrete in the arch; limestone and lime mortar in the spandrel walls in 1949 (Fig. 2(a)). In 2004, the bridge was restored to its state in the second half of the 19<sup>th</sup> century and the shops on it were rebuilt as wooden (Fig. 2(b)) [16, 22, 23].

The Irgandi Bridge is about 62 m long and 10.7 m wide, consists of one main arch with 7.37 m height and 15.05 m span, spandrel walls and backfill material. The thickness of massive concrete arch is 0.99 m at the crown (Fig. 3). The structure of the arch was made of massive concrete, while the spandrel walls were built with limestone and lime mortar. The shops on the bridge were constructed by using Scotch Pine.

Different modelling techniques have used to predict the seismic performance of masonry structures since the 1970s. In the early 1970s, 1D (one-dimensional) modelling method was used; but it was concluded that this modelling method did not demonstrate accurate stress distribution after cracking the masonry structures [24]. In the following years, 2D (two-dimensional) modelling approach was

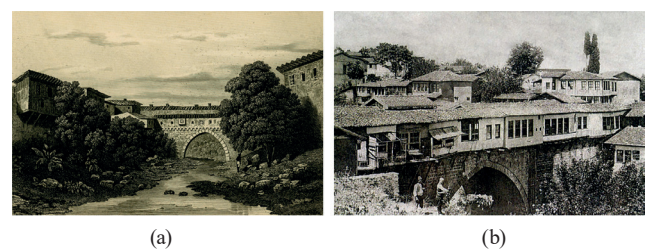


Fig. 1 Irgandi Bridge (a) before [20] and (b) after [21] the 1855 Bursa Earthquake



Fig. 2 Irgandi Bridge in (a) 1950s [22] and (b) Current state of the Bridge [23]

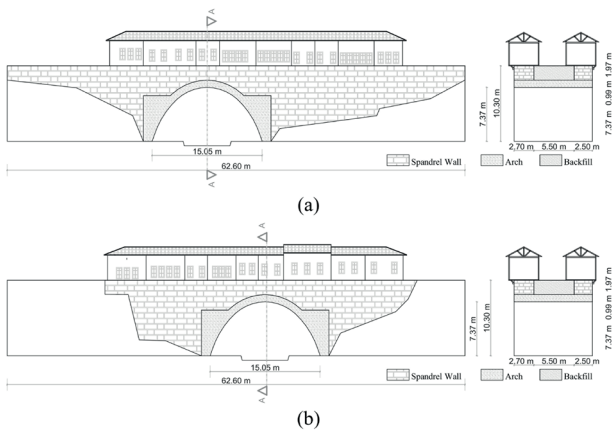


Fig. 3 Façade of Irgandi Bridge (a) Downstream façade, (b) Upstream façade

began to use, but realistic results in predicting the failure mechanism in asymmetrical bridges and arches were not obtained with this modelling method [25]. Finally, 3D (three-dimensional) modelling approach has been adopted as a more realistic modelling method. For this reason, 3D modelling technique was used in this study, in which the failure mechanism can be predicted more accurately.

Three different modeling methods are used in modeling masonry structures, namely detailed micro, simplified micro and macro modeling techniques (Fig. 4) [10, 17, 26–29]. In micro modeling technique, mortar material and masonry elements (stone or brick material) are modeled separately (Fig. 4(a)). In simplified micro-modelling, the dimensions of the masonry elements are expanded by half the thickness of the mortar material (Fig. 4(b)). Modeling is performed by defining specific contacts to the interface formed between the extended masonry elements [27].

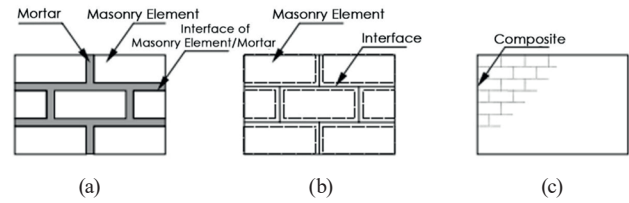


Fig. 4 Modelling methods for masonry structures (a) Detailed micro, (b) Simplified micro, (c) Macro [10, 17, 26–29]

Although detailed micro and simplified micro modeling techniques are useful and highly accurate in small-scale wall elements, they cause incorrect modeling and requires large computational capability and time in large-scale structures. In large-scale structures, when the mechanical properties and boundary conditions of materials are correctly defined, accurate results could be obtained with the macro model as close as the micro model [28]. In this context, macro modeling method is preferred to model the Irgandi Bridge in this study (Fig. 4(c)).

Façade views and shop sections of the Irgandi Bridge are shown in Fig. 3 and Fig. 5, respectively. The finite element model of the bridge is created using the ANSYS v15 [30] software. In the finite element model, the arch and vaults as first element, the spandrel walls as second element and the backfill and soil as third element of the bridge are modelled separately (Fig. 6). The bridge model is created by connecting these three different elements with bonded contact. The shops on the bridge are not created in the finite element model; the load of the shops is acted on the model using the distributed mass approach. Solid 65 is utilized as element type in the ANSYS software for the 3D finite element model and analyses of the bridge. The element is

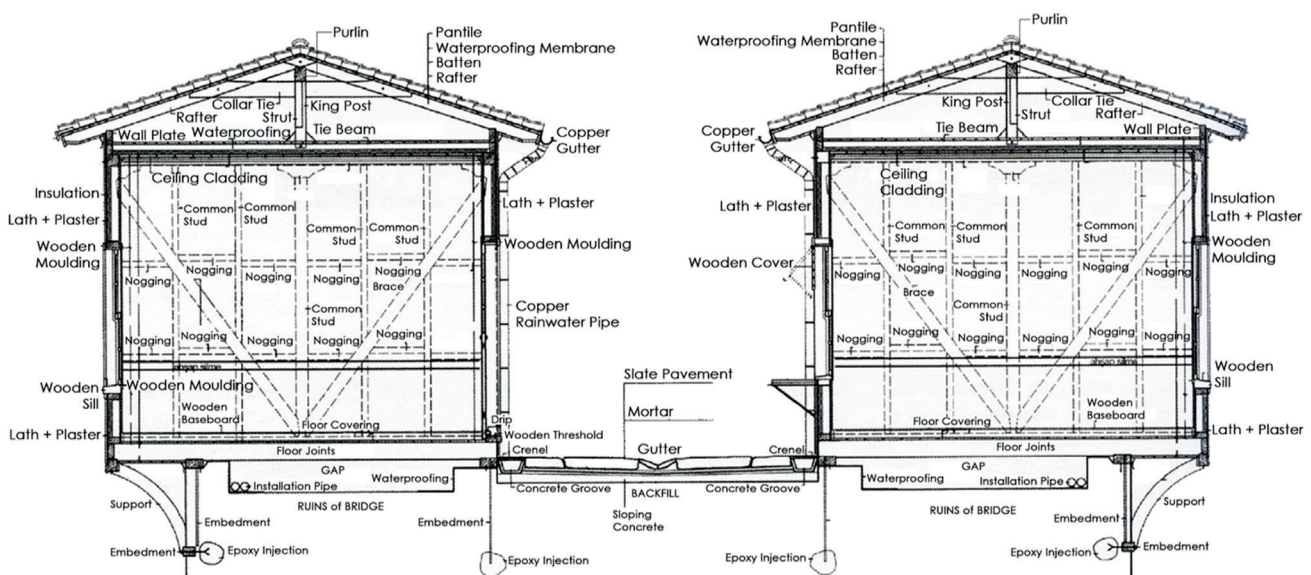


Fig. 5 Section of wooden shops on Irgandi Bridge [16, 17]

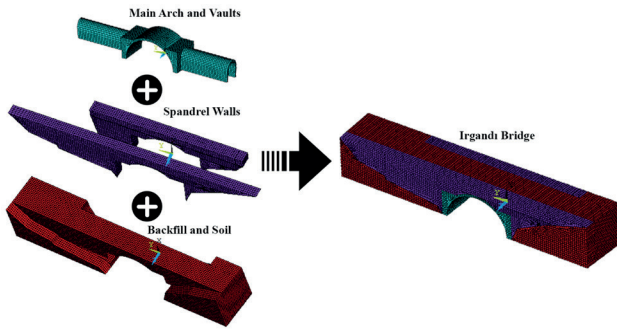


Fig. 6 Main arch, vaults, spandrel walls and backfill of Irgandi Bridge

defined by 8 nodes having three degrees of freedom per node. In the finite element mesh, 89969 nodal points and 86057 solid elements are used.

### 2.2 Material properties

The Irgandi Bridge consisted of a single arch and vaults made up of massive concrete, spandrel walls made up of limestone and lime mortar, backfill and soil. The compressive strength of concrete is taken as 33.5 MPa as mean of core samples were taken from the arch structure of Irgandi Bridge as part of the restoration conducted by Bursa Metropolitan Municipality in 2003 (Table 1) [17]. The Young's modulus and tensile strength of the massive concrete in the model are calculated using Eqs. (1)–(2), respectively [31]. In addition, density and Poisson's ratio of the massive concrete is taken as 2300 kg/m<sup>3</sup> and 0.2, respectively.

$$E_c = 4750\sqrt{f_c} \quad (1)$$

$$f_{ct} = 0.63\sqrt{f_c} \quad (2)$$

where  $E_c$  refers to Young's modulus of concrete,  $f_c$  refers to compressive strength of concrete,  $f_{ct}$  refers to tensile strength of concrete.

Since it is not possible to take samples from the historical bridge for the mechanical properties of limestone and lime mortar materials, the values frequently used in the literature have been taken into account. The compressive strengths of limestone and lime mortar are taken as 45 MPa and 1.24 MPa, respectively [32]. In order for these material properties to be used in macro modelling method, the materials are homogenized using Eqs. (3)–(6) [33]. In the study, the tensile strength of the homogenized masonry element is used as 10% of the compressive strength [15, 34]. The volumetric ratio of the masonry element and the mortar are taken as 90% and 10%, respectively. The mechanical properties of the homogenized material considered within the scope of the study are presented in Table 2.

$$f_{mas} = 0.6f_b^{0.65}f_m^{0.25} \quad (3)$$

$$E_{mas} = 1000f_{mas} \quad (4)$$

$$\Upsilon_{mas} = \Upsilon_bV_b + \Upsilon_mV_m \quad (5)$$

$$v_{mas} = v_bV_b + v_mV_m \quad (6)$$

where  $f$  refers to the compressive strength,  $E$  refers to Young's modulus,  $\Upsilon$  refers to the density,  $V$  refers to the volume,  $v$  refers to Poisson's ratio. Additionally, the subscript  $mas$  refers to the homogenized masonry structure, the subscript  $b$  refers to brick or stone, the subscript  $m$  refers to the mortar.

In order to take into account, the nonlinear material properties of both masonry elements and massive concrete, the three-parameter yield criterion developed by Willam and Warnke [35] is used. The yield criterion could take into account both cracks and crushing that occur in the material under multiaxial stress state. In the yield criterion, the yield surface is defined using principal stresses and five different parameters. In the elements exceeding the yield surface, cracks occur due to tensile stress or crushing due to compressive stress. Shear transfer coefficients for open and closed cracks must be defined to determine the yield surface. The shear stress transfer coefficients are considered as 0.2 and 0.8 for massive concrete, respectively [36–38] and the coefficients are considered 0.01 both open and close cracks for masonry elements [28, 39]. The reason why shear stress transfer coefficients are chosen as 0.01 in the masonry element is to ensure stability in the model.

Table 1 Core samples of the arch

Sample No	Compressive Strength (MPa)
1	34.0
2	40.0
3	23.9
4	40.2
5	35.8
6	31.8
7	27.8
8	34.5
Mean Value	33.5

Table 2 Material properties of spandrel walls

Element of structure	Density (kg/m <sup>3</sup> )	Poisson's ratio	Young's modulus (MPa)	Compressive Strength (MPa)
Spandrel walls	2510	0.29	7518	7.52



Values in the literature is used for backfill and soil material mechanical properties, given in Table 3 [15, 40]. In addition, Drucker-Prager material model is used for backfill material and soil.

**2.3 Operational modal analysis (OMA)**

Operational Modal Analysis (OMA) test method is used to obtain the dynamic parameters of the structures. Natural vibration frequencies, damping ratios and mode shapes can be find out by using this non-destructive test method.

The dynamic parameters of structures from output-only experimental data can be find in this technique. The loads are environmental forces and the modal identification based on responses only. 2400 mV/g highly sensitive accelerometers are used in tests. Monoaxial accelerometers which have 0.01–200 Hz bandwidths and ±3 g measurements range are used in this study. Testbox 2010 data acquisition device which has 8 channels is used in dynamic tests [18].

For the accuracy of tests, 30-minute test periods are applied. Accelerometers are placed in the direction of river flow and vertical direction on the bridge. Orientation of sensors and the test setup are presented on the plan layout and the section view of Irgandi Bridge in Fig. 7.

The sensor orientations are carefully checked and fixed on the ground of the bridge at river flow and vertical directions in front of the timber houses (Fig. 8). The natural frequencies, mode shapes and damping ratios of the bridge

are identified by using Frequency Domain Decomposition (FDD) and Peak Picking (PP) methods. After the test setup results are examined, it is observed that the first frequencies occurred in river flow direction at 11.91 Hz. In addition, the first frequency in the vertical direction is determined as 18.97 Hz. The singular values of the spectral densities for the first modes in river flow and vertical direction can be seen in Fig. 9. It is determined that the damping ratio in the flow direction and vertical direction is 7.67% and 4.68%, respectively.

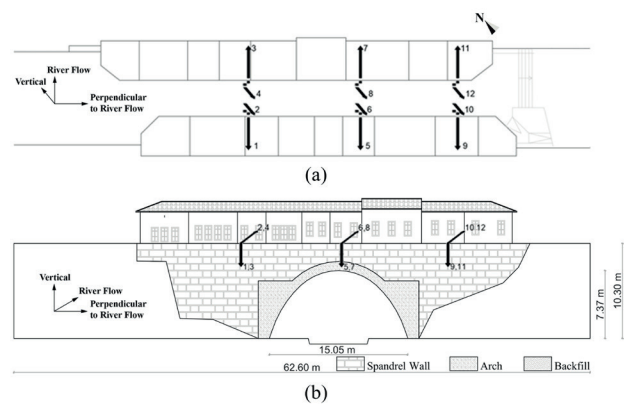


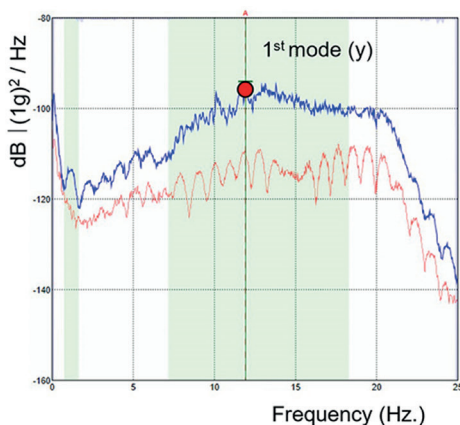
Fig. 7 The sensor orientations (a) Plan layout, (b) Section view



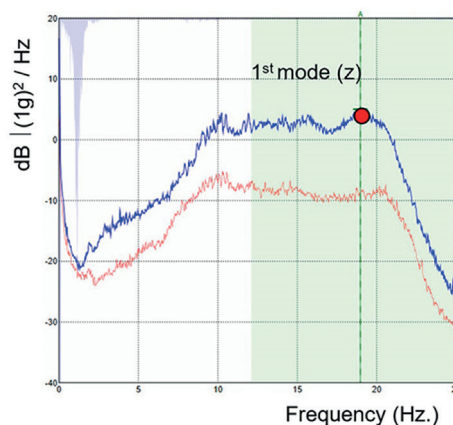
Fig. 8 Vibration tests (a) Sensor placements on the bridge (b) Direction of sensors

Table 3 Material properties of backfill and soil

Element of structure	Density (kg/m <sup>3</sup> )	Poisson's ratio	Young's modulus (MPa)	Cohesion (MPa)	Friction angle (°)
Backfill and soil	1800	0.20	500	0.05	20



(a)



(b)

Fig. 9 The singular values of the spectral densities (a) 1<sup>st</sup> mode in flow direction (b) 1<sup>st</sup> mode in vertical direction

### 2.4 Finite element model updating

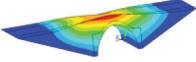
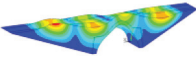
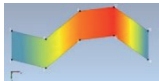
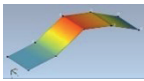
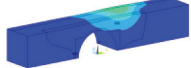
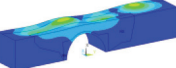
Different damages may occur in long-term lifespan of masonry structures. This situation causes difficulties in accurately transferring the dynamic behavior of masonry structures to the finite element model. It is necessary to update the numerical model to minimize the differences between the experimental tests and the numerical model.

Manual and automatic updating approaches are used in the validation of masonry structures [41]. In this study, manual updating method is used. Manual updating is based on validating the numerical model by trial-and-error method depending on the support condition, material properties and geometry of the structure. If the difference between the experimental model and the numerical model is less than 5% as result of the update, it is assumed that the dynamic characteristics of the numerical model are accurately demonstrated (Fig. 10).

In this context, the idealized model of the Irgandi Bridge by Sakcali et al. [17] and the mode results obtained as result of OMA are compared (Table 4). While the frequency values of the first mode and the sixth mode obtained as a result of OMA are 11.91 Hz and 18.97 Hz, respectively, these values in the idealized model are determined to be 25.4% and 36.1% higher, respectively.

For this reason, the model is created that considers the soil-structure interaction instead of the idealized model. In addition, the stiffness of the spandrel walls affects the structural characteristic of the bridge [42, 43]. So, the geometry of the spandrel walls is remodeled instead of idealized spandrel walls. The created model is updated depending on

**Table 4** Updating of the numerical model

Behavior (Mode number)	First bending mode for direction parallel to the river flow (Mode 1)	First vertical asymmetric mode (Mode 6)
Idealized model [17]	 14.94 Hz	 25.81 Hz
Operational Modal Analysis (OMA)	 11.91 Hz	 18.97 Hz
Model Considering Soil-Structure Interaction	 11.94 Hz	 19.02 Hz

the OMA results. It is determined that there is a 0.26% difference in the first mode and sixth mode frequency values of the updated model and OMA. In this context, it is determined that the results of experimental tests and the model, in which the soil-structure interaction is taken into account, are very compatible (Table 4). The reasons for considering the soil-structure interaction model are that the vaults and spandrel walls of the bridge lay directly on the ground, as well as the variable geometries of the spandrel walls cause convergence problems in the model.

In the study, it is established that the effective mass participation of the first 25 modes of the finite element model, whose soil-structure interaction is taken into account, is 95%. Moreover, it is determined that these modes change in the range of 11.94–28.47 Hz. 5% damping ratio is taken

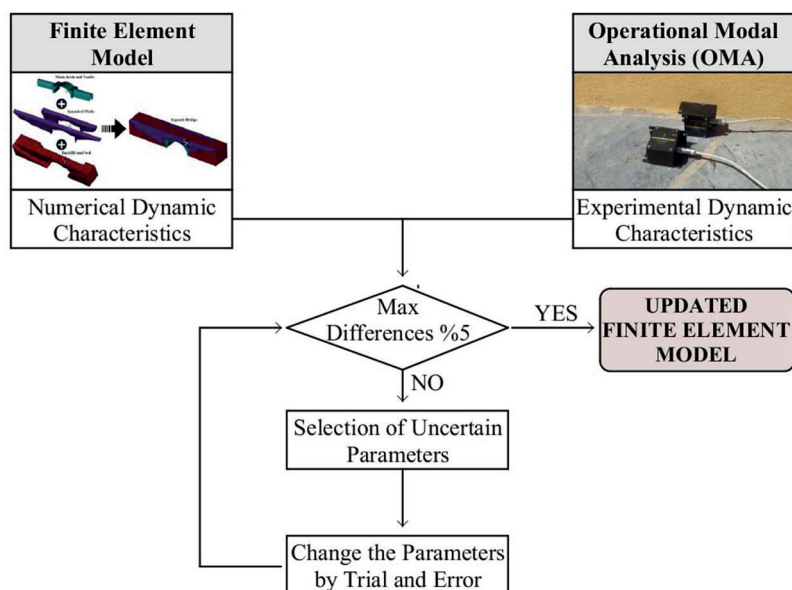


**Fig. 10** FEM manual updating procedure

in the study considering the damping ratios obtained from the experimental tests are in the range of 7.67–4.68%. Rayleigh Damping Coefficient is used to consider the dynamic energy loss and different modes in the model. Mass (Eq. (7)) and stiffness (Eq. (8)) matrix multipliers [44] are calculated as 5.284 and 0.000394, respectively, and used in the study.

$$\alpha = 2\xi \frac{\omega_{min}\omega_{max}}{\omega_{min} + \omega_{max}}, \quad (7)$$

$$\beta = \frac{2\xi}{\omega_{min} + \omega_{max}}, \quad (8)$$

where  $\alpha$  is the factor of mass proportional damping,  $\beta$  is the factor of stiffness proportional damping,  $\xi$  is damping ratio,  $\omega_{min,max}$  are the angular frequency values.

### 2.5 Artificial earthquake records

Two artificial earthquake records perpendicular to each other are created for three different earthquake levels (DD-1, DD-2, DD-3) for the dynamic analysis of the Irgandi Bridge [45]. According to BECT-2018 [46] DD-1, DD-2 and DD-3 earthquake levels denotes respectively very rare earthquake with a recurrence period of 2475 years (2% probability of exceedance in 50 years), rare earthquakes with a recurrence period of 475 years (10% probability of exceedance in 50 years) and frequent earthquake with a recurrence period of 72 years (50% probability of exceedance in 50 years). It has been determined that the soil on which the bridge sits is poorly weathered, medium solid rock class (Local Soil Classification: ZB) [46].

Depending on these parameters, elastic spectrum acceleration graphs for three different earthquake levels of the region are presented in Fig. 11. The PGA (Peak Ground Acceleration) values for the three earthquake levels are

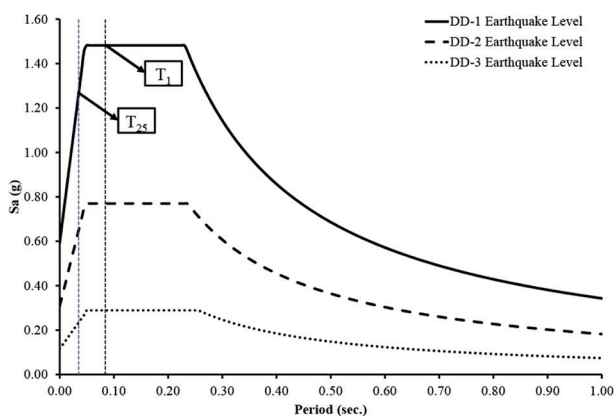


Fig. 11 Elastic spectrum acceleration graphs of DD-1, DD-2 and DD-3 earthquake levels

0.664 g, 0.356 g and 0.138 g, respectively. Artificial acceleration-time graph performed in the direction of flow and perpendicular to the flow direction are presented in Fig 12. The acceleration records are obtained by using SeismoArtif software [47]. While creating the artificial earthquake record, it is considered that it should not be less than 5 times the first natural vibration period of the structure and not shorter than 15 seconds [48]. In this study, Saragoni and Hart Function is used to obtain the acceleration records, and the total earthquake recording time is chosen as 20 seconds [49].

## 3 Results and discussion

### 3.1 Comparative analysis of linear and nonlinear dynamic analysis under DD-3 earthquake level

Displacement-time history graph of linear and nonlinear dynamic analysis of Irgandi Bridge in flow direction of 2478 node for DD-3 earthquake level is presented in Fig. 13. As a result of the nonlinear dynamic analysis for the DD-3 earthquake level, no damage zone occurs. In addition, as a result of linear and nonlinear dynamic analysis, it is determined that the maximum displacement at the node 2478 (at the 6<sup>th</sup> second) is 0.49 mm and 0.51 mm, respectively. It is detected that since no damage zones occurs in nonlinear dynamic analysis, the similar results as linear dynamic analysis is obtained. In addition, crack propagation is not investigated since no damage zone occurs at the earthquake level.

### 3.2 Comparative analysis of linear and nonlinear dynamic analysis under DD-2 earthquake level

Displacement-time history graph of linear and nonlinear dynamic analysis of Irgandi Bridge in flow direction of 2478 node for DD-2 earthquake level is presented in Fig. 14. As a result of linear and nonlinear dynamic analysis, it is determined that the maximum displacement at the node 2478 (at the 6<sup>th</sup> second) are 1.35 mm and 1.78 mm, respectively. As a result of the nonlinear dynamic analysis for the DD-2 earthquake level, damage zones occur. Therefore, the stiffness of the system decreases in nonlinear dynamic analysis and the displacement in nonlinear dynamic analysis is typically 30-35% more than in linear dynamic analysis.

The damage zones of the Irgandi Bridge, which nonlinear dynamic analysis is performed at the DD-2 earthquake level, are given in Fig. 15. The first crack for the DD-2 earthquake level occurs in the 2.25<sup>th</sup> second at the end of the upstream façade support region. In the 6<sup>th</sup> second,

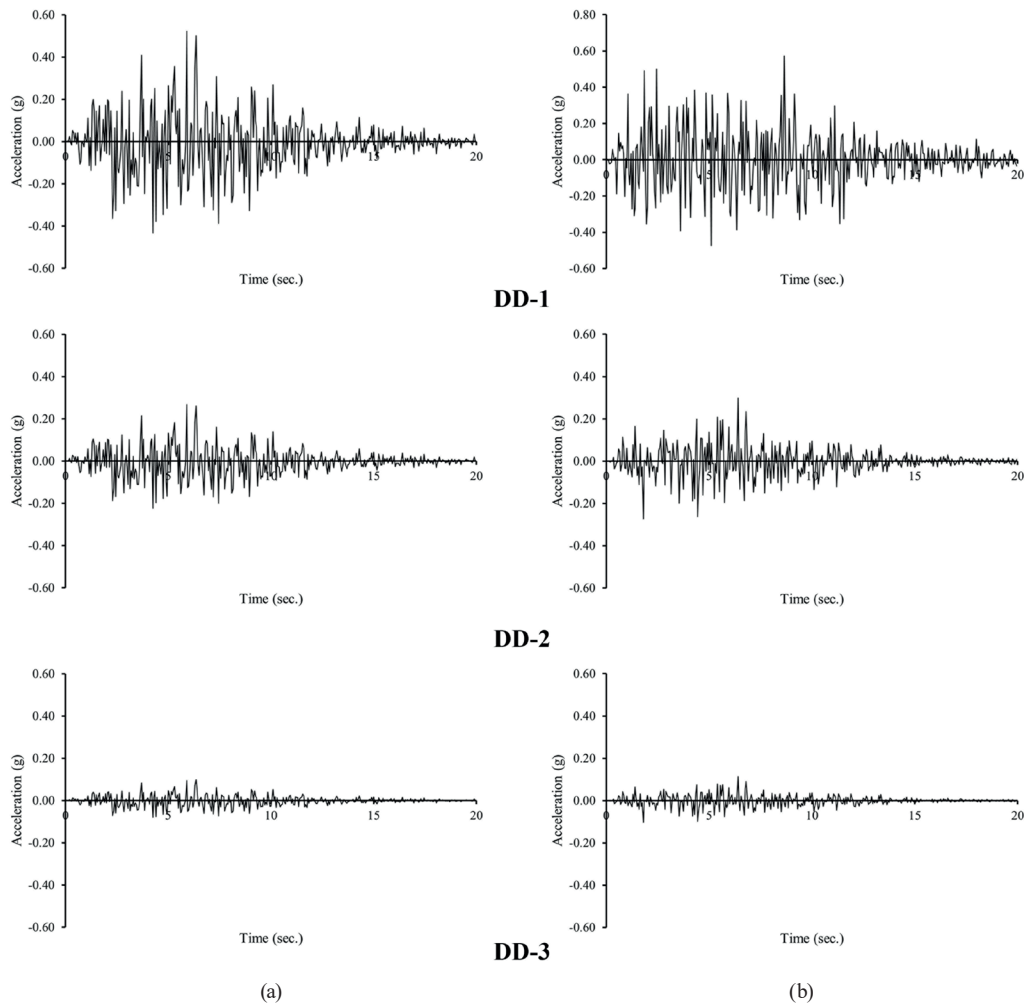


Fig. 12 Artificial acceleration-time graph for different earthquake level (a) Flow direction, (b) Perpendicular to the direction of flow

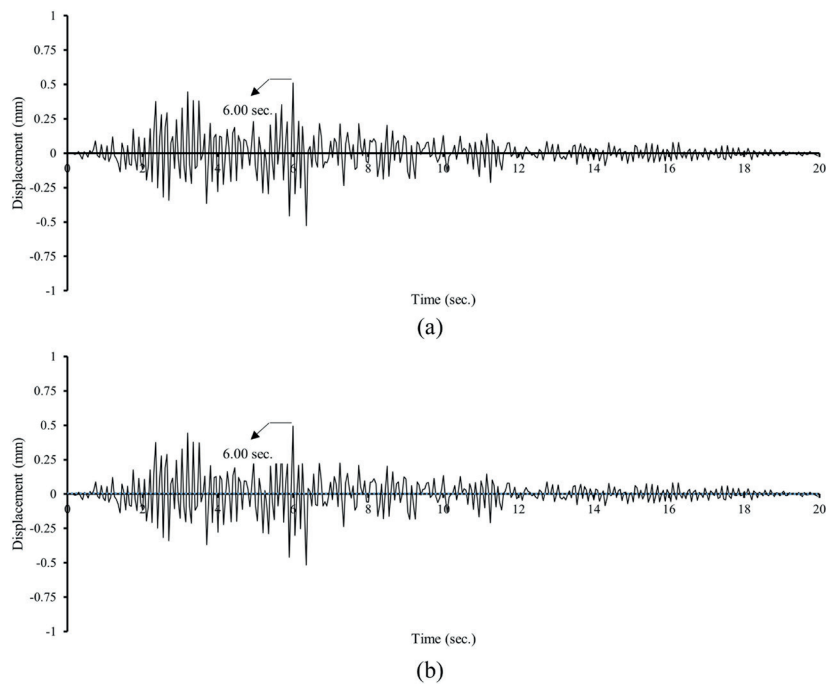
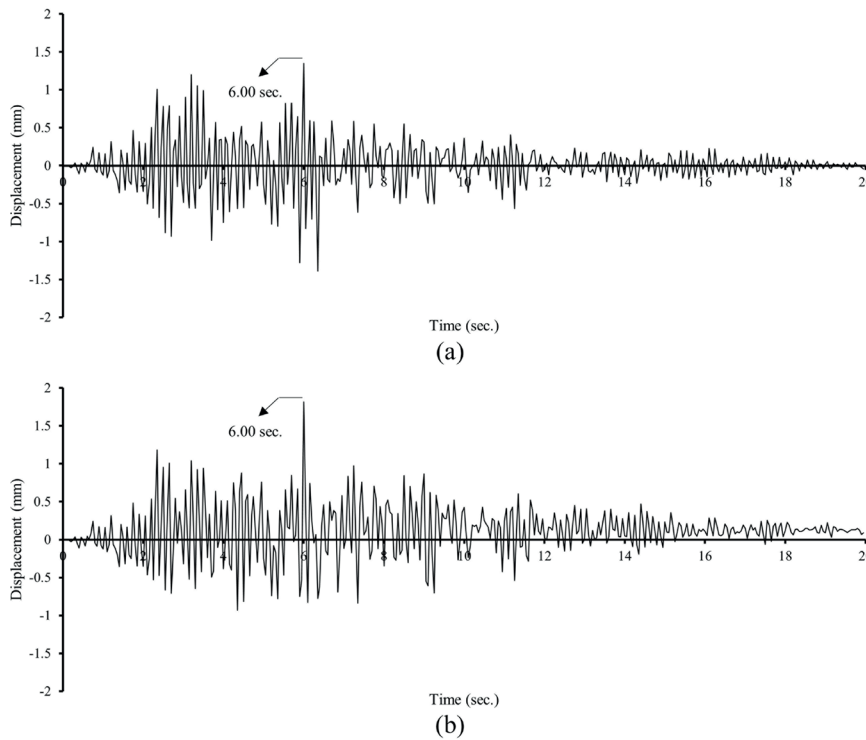
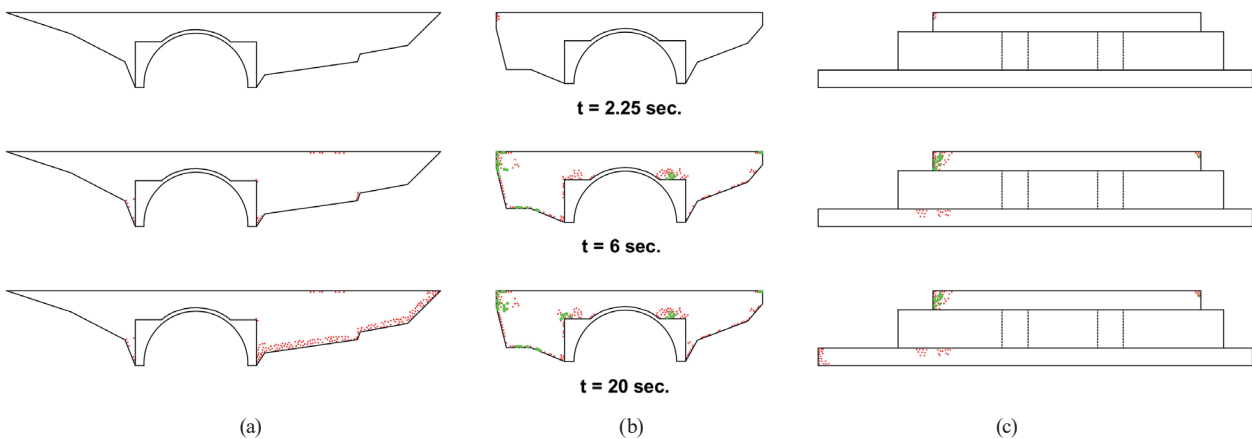


Fig. 13 Displacement-time history graph in flow direction of 2478 node for DD-3 earthquake level (a) Linear dynamic analysis, (b) Nonlinear dynamic analysis





**Fig. 14** Displacement-time history graph in flow direction of 2478 node for DD-2 earthquake level (a) Linear dynamic analysis, (b) Nonlinear dynamic analysis



**Fig 15** Damage zones of Irgandi Bridge for DD-2 earthquake level (a) Downstream façade, (b) Upstream façade, (c) Plan layout

when the system reaches the maximum displacement, cracks occur on the left support and arch joint region of the upstream façade. Cracks also begin to occur in the right support region of the downstream façade. Furthermore, damage zones in the spandrel wall of the upstream façade progress. At the final state (20<sup>th</sup> second), damage zones in the spandrel walls of upstream façade and the support regions of downstream façade occur. In addition, no damage is observed in the massive concrete arch at the DD-2 earthquake level.

### 3.3 Comparative analysis of linear and nonlinear dynamic analysis under DD-1 earthquake level

Displacement-time history graph of linear and nonlinear dynamic analysis of Irgandi Bridge in flow direction of 2478 node for DD-1 earthquake level is presented in Fig. 16. As a result of linear dynamic analysis, it is determined that the maximum displacement at the node 2478 (at the 6<sup>th</sup> second) is 2.71 mm. Since cracks and crushing are taken into account in the nonlinear dynamic analysis, this situation causes a decrease in the system stiffness. For this reason, the maximum displacement in nonlinear

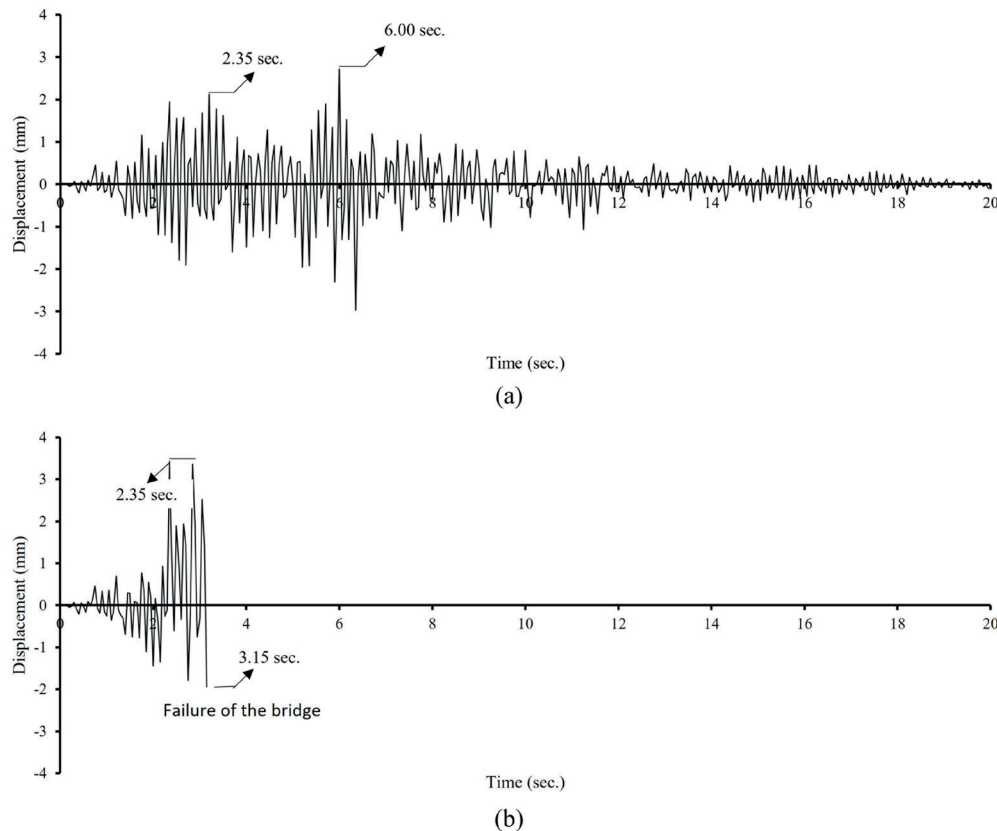


**Fig. 16** Displacement-time history graph in flow direction of 2478 node for DD-1 earthquake level (a) Linear dynamic analysis, (b) Nonlinear dynamic analysis

dynamic analysis is detected to be 3.43 mm at the 2.35<sup>th</sup> second. The displacement is detected to be 1.94 mm in the linear dynamic analysis at this moment. It is determined that the displacement obtained as a result of the nonlinear dynamic analysis is typically 75–80% more than the linear dynamic analysis.

As a result of linear dynamic analysis of the Irgandi Bridge for the DD-1 earthquake level, the maximum and minimum principal stress state at 1.2<sup>nd</sup> second, 2.35<sup>th</sup> second and 6<sup>th</sup> second are given in Fig. 17. According to nonlinear dynamic analysis, the first crack occurs in the bridge at 1.2<sup>nd</sup> second. At the same time phase, as a result of linear dynamic analysis, it is determined that the maximum principal stress is 1.02 MPa. The stress occurs both in the massive concrete arch and spandrel walls of upstream façade. However, the tensile strength of massive concrete is 3.65 MPa. So, it is determined that the maximum principal stress is not exceeded in massive concrete. However, the fact that the tensile strength of the homogenized material of spandrel walls is 0.752 MPa demonstrates that cracks will occur in the support region of the spandrel walls. This situation is similar to the results of nonlinear analysis. At the 2.35<sup>th</sup> second, the stress level in spandrel walls increases

up to 3.68 MPa. It is observed that the maximum principal stresses in some parts of the spandrel walls of upstream façade exceed the tensile strength of homogenized material. It is also observed that the maximum principal stress is exceeded in the lower parts of the massive concrete arch. Although this situation is similar to nonlinear analysis, the failure mechanism is occurred at 3.15<sup>th</sup> second as a result of nonlinear analysis. Since a failure mechanism is not detected in the linear analysis, the principal stresses at the 6<sup>th</sup> second, when the maximum displacement of the linear analysis occurred, are also examined. As a result of this examination, it is determined that the maximum and minimum principal stress values reached the highest level in the bridge at the 6<sup>th</sup> second. It is also observed that while the tensile strengths are exceeded in some region of the massive concrete arch and the spandrel walls, the compressive strengths are not exceeded. Furthermore, it can be determined whether there is any damage to the bridge by examining the maximum and minimum principal stresses in the linear dynamic analysis at the moment of the maximum displacement of the bridge. However, it is not possible to make an estimation as to whether the system will reach failure mechanism or not.

The damage zones of the Irgandi Bridge, which nonlinear dynamic analysis is performed at the DD-1 earthquake level, are given in Fig. 18. The first crack for the DD-1 earthquake level occurs in the 1.2<sup>nd</sup> second at the end of the upstream façade support region. In the 1.75<sup>th</sup> second, it is observed that severely damage zones occur in the right support region of the same façade and gradually in the upper left region of the arch. Cracks also begin to occur in the spandrel wall support region of the downstream façade. By the 2.35<sup>th</sup> second, it is observed that damage

zones occur in all the support region. Between the 2.35<sup>th</sup> and 2.85<sup>th</sup> seconds, it is observed that damage zones progress in the upper left corner of the arch in the plan view. The damage zones coalesce and the system reaches labile at 3.15<sup>th</sup> seconds. After this stage, the convergence cannot be provided in the numerical model, since the system is damaged. Thus, it can be assumed that the failure mechanism has occurred. The predicted failure mechanism of the bridge in the downstream façade, upstream façade and plan views are presented in Fig. 19.

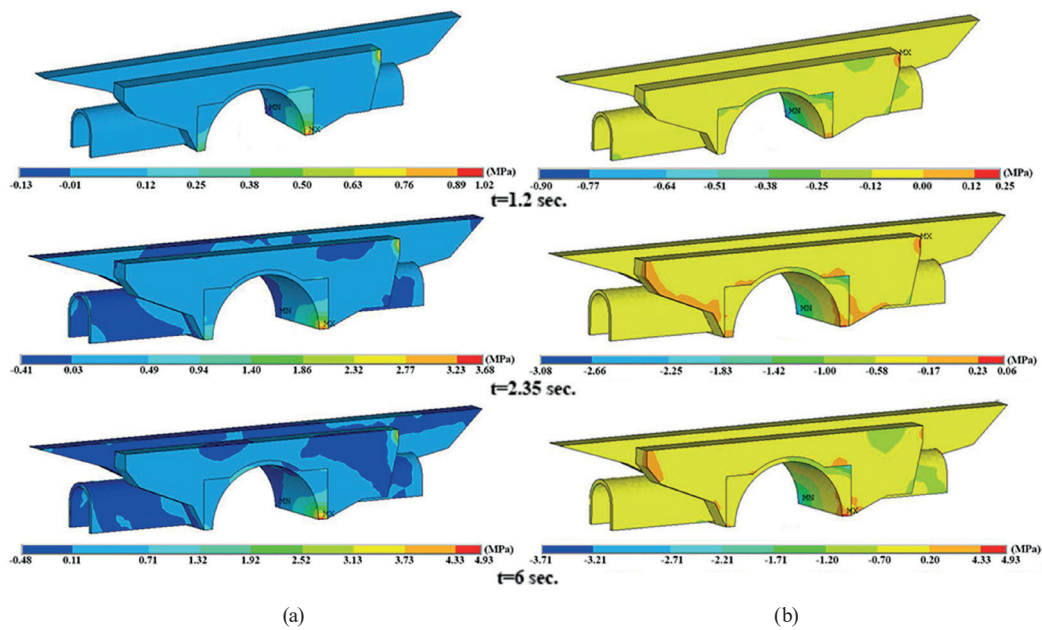


Fig 17 Principal stress contours of Irgandi Bridge for DD-1 earthquake level and linear dynamic analysis (a) Maximum principal stress, (b) Minimum principal stress

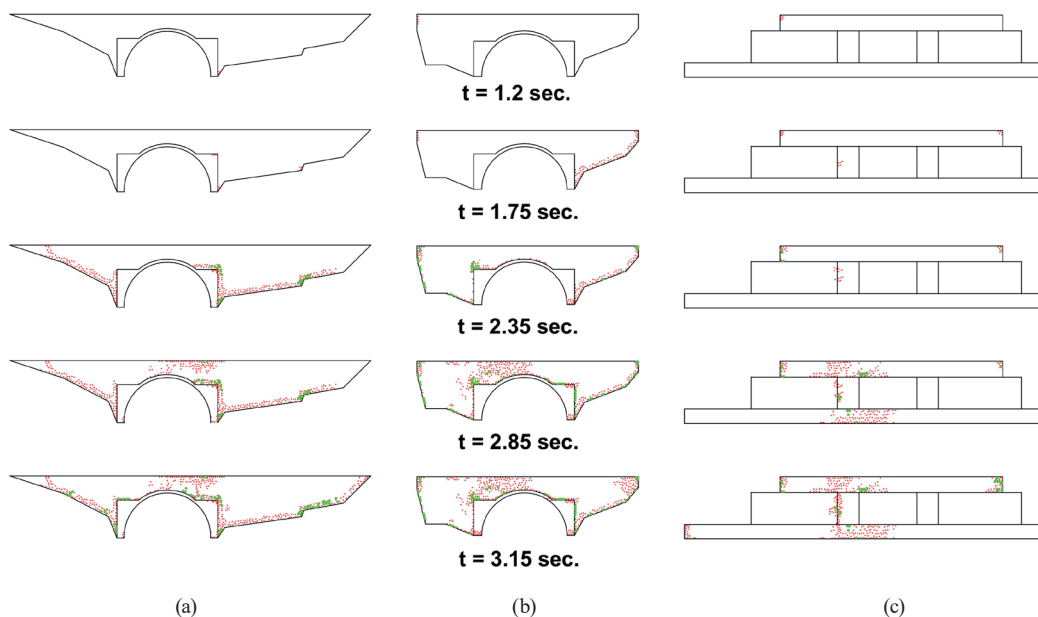


Fig. 18 Damage zones of Irgandi Bridge for DD-1 earthquake level (a) Downstream façade, (b) Upstream façade, (c) Plan layout

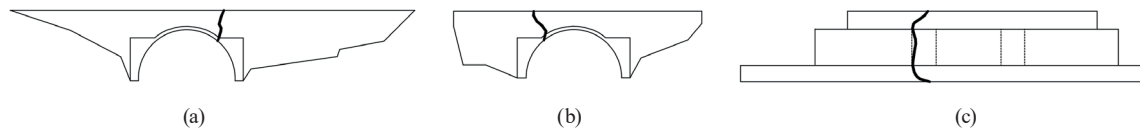


Fig. 19 Failure mechanisms of Irgandi Bridge for DD-1 earthquake level (a) Downstream façade, (b) Upstream façade, (c) Plan layout

#### 4 Conclusions

Irgandi Bridge, which is one of the few historical bridges in the world with shops on it, was first built in 1442 and finally restored to its state in the second half of the 19<sup>th</sup> century in 2004. The bridge spans over the Gökdere River in the city of Bursa, is about 62 m long and 10.7 m wide and consists of one main arch with 7.37 m height and 15.05 m span.

The earthquake behavior and failure mechanism of the Irgandi Bridge are investigated in this study. In this context, the finite element model of the Irgandi Bridge is created considering the soil-structure interaction and this model is updated by taking into account tests performed with the OMA method on the bridge. Both of linear and nonlinear dynamic analyses of the updated model are performed using the artificial records at three different earthquake levels created according to the region where the Irgandi Bridge is located. Since there is no crack occurred in the structural system at the DD-3 earthquake level, there was no change in system stiffness as a result of nonlinear dynamic analysis. Accordingly, no significant difference is observed in time-dependent displacements as a result of linear and nonlinear dynamic analysis. However, damage

zones occur in the Irgandi Bridge for DD-1 and DD-2 earthquake levels. Although the system does not reach the failure mechanism for the DD-2 earthquake level, there is a decrease in system stiffness because of damage zones. This situation causes the maximum displacement in nonlinear dynamic analysis to be typically 30–35% more than in linear dynamic analysis. If the Irgandi Bridge is exposed to an earthquake of DD-1 earthquake level, since damage zones occurs, stiffness of the system decreases as same for DD-2 earthquake level. In addition, damage zones primarily occur in the support region of the Irgandi Bridge. Under the loads of DD-1 earthquake level, the damage zones coalesce and the system reaches the failure mechanism in 3.15<sup>th</sup> second. For this reason, viewed from the upstream façade, the upper left corner of the bridge arch should be strengthened. According to the results, the computational capability and time could be reduced by using linear dynamic analysis in such masonry structures exposed to low level earthquake such as DD-3. However, it is predicted that nonlinear dynamic analysis will give more accurate results when the system is exposed to earthquake levels such as DD-1 or DD-2.

#### References

- [1] Yılmaz, C., Caner, A., Turer, A. "Bridge Engineering in Turkey", In: Chen, W., Duan, L. (eds.). Handbook of International Bridge Engineering, CRC Press, 2013, pp. 842–883. ISBN 9780429093456
- [2] Pérez-Gracia, V., Di Capua, D., Caselles, O., Rial, F., Lorenzo, H., González-Drigo, R., Armesto, J. "Characterization of a Romanesque Bridge in Galicia (Spain)", International Journal of Architectural Heritage, 5(3), pp. 251–263, 2011.  
<https://doi.org/10.1080/15583050903560249>
- [3] Karaton, M., Aksoy, H. S. "Seismic damage assessment of an 891 years old historic masonry mosque", Periodica Polytechnica Civil Engineering, 62(1), pp. 126–135, 2018.  
<https://doi.org/10.3311/PPci.10270>
- [4] Maraş, M. M., Özmen, A., Sayın, E., Ayaz, Y. "Seismic assessment of the historical Sütlu Minaret Mosque", Periodica Polytechnica Civil Engineering, 66(2), pp. 445–459, 2022.  
<https://doi.org/10.3311/PPci.19400>
- [5] Hökelekli, E., Demir, A., Ercan, E., Nohutçu, H., Karabulut, A. "Seismic assessment in a historical masonry minaret by linear and non-linear seismic analyses", Periodica Polytechnica Civil Engineering, 64(2), pp. 438–448, 2020.  
<https://doi.org/10.3311/PPci.15126>
- [6] Fanning, P. J., Boothby, T. E. "Three-dimensional modelling and full-scale testing of stone arch bridges", Computers & Structures, 79(29–30), pp. 2645–2662, 2001.  
[https://doi.org/10.1016/S0045-7949\(01\)00109-2](https://doi.org/10.1016/S0045-7949(01)00109-2)
- [7] Brencich, A., Sabia, D. "Experimental identification of a multi-span masonry bridge: The Tanaro Bridge", Construction and Building Materials, 22(10), pp. 2087–2099, 2008.  
<https://doi.org/10.1016/j.conbuildmat.2007.07.031>
- [8] Altunisik, A. C., Kanbur, B., Genc, A. F., Kalkan, E. "Structural response of historical masonry arch bridges under different arch curvature considering soil-structure interaction", Geomechanics and Engineering, 18(2), pp. 141–151, 2019.  
<https://doi.org/10.12989/gae.2019.18.2.141>
- [9] Hökelekli, E., Yılmaz, B. N. "Effect of cohesive contact of backfill with arch and spandrel walls of a historical masonry arch bridge on seismic response", Periodica Polytechnica Civil Engineering, 63(3), pp. 926–937, 2019.  
<https://doi.org/10.3311/PPci.14198>
- [10] Özmen, A., Sayın, E. "Seismic response of a historical masonry bridge under near and far-fault ground motions", Periodica Polytechnica Civil Engineering, 65(3), pp. 946–958, 2021.  
<https://doi.org/10.3311/PPci.17832>



- [11] Aoki, T., Sabia, D., Rivella, D., Komiyama, T. "Structural characterization of a stone arch bridge by experimental tests and numerical model updating", *International Journal of Architectural Heritage*, 1(3), pp. 227–250, 2007.  
<https://doi.org/10.1080/15583050701241208>
- [12] Altunişik, A. C., Bayraktar, A., Sevim, B., Birinci, F. "Vibration-based operational modal analysis of the Mikron Historic Arch Bridge after restoration", *Civil Engineering and Environmental Systems*, 28(3), pp. 247–259, 2011.  
<https://doi.org/10.1080/10286608.2011.588328>
- [13] Costa, C., Arêde, A., Costa, A., Caetano, E., Cunha, Á., Magalhães, F. "Updating numerical models of masonry arch bridges by operational modal analysis", *International Journal of Architectural Heritage*, 9(7), pp. 760–774, 2015.  
<https://doi.org/10.1080/15583058.2013.850557>
- [14] Conde, B., Ramos, L. F., Oliveira, D. V., Riveiro, B., Solla, M. "Structural assessment of masonry arch bridges by combination of non-destructive testing techniques and three-dimensional numerical modelling: Application to Vilanova Bridge", *Engineering Structures*, 148, pp. 621–638, 2017.  
<https://doi.org/10.1016/j.engstruct.2017.07.011>
- [15] Karaton, M., Aksoy, H. S., Sayın, E., Calayır, Y. "Nonlinear seismic performance of a 12th century historical masonry bridge under different earthquake levels", *Engineering Failure Analysis*, 79, pp. 408–421, 2017.  
<https://doi.org/10.1016/j.engfailanal.2017.05.017>
- [16] Eyüpgiller, K. K., Ersen, A., Özgen, K. "Irgandı Bridge restoration and reconstruction implementation", *Yapı Dergisi*, 273, pp. 75–80, 2004. (in Turkish)
- [17] Sakcalı, G. B., Gönül, A., Yüksel, İ. "Seismic behavior of historical masonry bridges: The case study of Irgandı Bridge", *International Journal of Architectural Engineering Technology*, 6(1), pp. 24–32, 2020.  
<https://doi.org/10.15377/2409-9821.2019.06.4>
- [18] Structural Vibration Solution "Operational modal analysis, (Release 4.5)", 2016. [software] Available at: <https://svibs.com/applications/operational-modal-analysis/>
- [19] Önge, Y. "The original architecture of the Irgandı Bridge in Bursa", *Vakıflar Dergisi*, 13, pp. 425–448, 1981. (in Turkish)
- [20] Texier, C. "Description de l'Asie mineure: Beaux-Arts, monuments historiques, plans et topographie des cités antiques; faite par ordre du Gouvernement Français" (Description of Asia Minor: Fine Arts, historical monuments, plans and topography of ancient cities; made by order of the French Government), Firmin Didot Frères, 1839. (in French)  
<https://doi.org/10.11588/diglit.4674>
- [21] Diez, E., Glück, H. "Alt-Konstantinopel: Hundertzehn photographische Aufnahmen der Stadt und ihrer Bau- und Kunstdenkmäler; mit alten Ansichten und Plänen sowie einer geschichtlichen Einleitung" (Old Constantinople: One hundred and ten photographs of the city and its architectural and artistic monuments; with old views and plans as well as a historical introduction), Roland-Verlag, Munich, Germany, 1920. (in German)
- [22] Celal, E. "Bursa - Old Photos" [online] Available at: <http://wowturkey.com/forum/viewtopic.php?p=8587043> [Accessed: 15 April 2022]
- [23] Bursa Metropolitan Municipality "Irgandı Köprüsü'ne turistik düzenleme" (Touristic arrangement for Irgandı Bridge), (in Turkish) [online] Available at: <https://www.bursa.bel.tr/haber/irgandi-koprune-turistik-duzenleme--29273> [Accessed: 15 April 2022]
- [24] Rouf, M. A. "Fundamental properties of brickwork with particular emphasis to brickwork arches", PhD Thesis, University of Liverpool, 1984.
- [25] Zhang, Y. "Advanced nonlinear analysis of masonry arch bridges", PhD Thesis, Imperial College London, 2014.
- [26] Lourenço, P. B. "Computational strategies for masonry structures", PhD Thesis, Delft University of Technology, 1996.
- [27] Sakcalı, G. B., Gönül, A., Parlak, I. E. "The Structural Behavior of Bridge Arches Under Collapse Load", *Journal of Polytechnic*, 23(4), pp. 929–939, 2020.  
<https://doi.org/10.2339/politeknik.633173>
- [28] Sakcalı, G. B., Öztürk, Y., Çelik, İ. D., Davraz, M. "The effect of new generation polyurethane wall block on single span steel frame behavior", *Journal of Building Engineering*, 48, 103986, 2022.  
<https://doi.org/10.1016/j.jobte.2021.103986>
- [29] Özmen, A., Sayın, E. "Seismic assessment of a historical masonry arch bridge", *Journal of Structural Engineering & Applied Mechanics*, 1(2), pp. 95–104, 2018.  
<https://doi.org/10.31462/jseam.2018.01095104>
- [30] Swanson Analysis Systems Inc., ANSYS "Finite Element Software", 2013. [software] Available at: <https://www.ansys.com/> [Accessed: 15 April 2022]
- [31] ACI Committee "Building code requirements for structural concrete (ACI 318-95) and commentary (318R-95)", American Concrete Institute, MI, USA, 1995.
- [32] Look, B. G. "Handbook of Geotechnical Investigation and Design Tables", Taylor & Francis, 2007. ISBN 9780203946602.  
<https://doi.org/10.1201/9780203946602>
- [33] WP4 Participants "Guideline for Load and Resistance Assessment of Existing European Railway Bridges - Advices on the Use of Advanced Methods (SB-LRA)", European Commission, Gothenburg, Sweden, 2006.
- [34] Kahraman, S., Fener, M., Kozman, E. "Predicting the compressive and tensile strength of rocks from indentation hardness index", *Journal of the Southern African Institute of Mining and Metallurgy*, 112(5), pp. 331–339, 2012.
- [35] Willam, K. J., Warnke, E. P. "Constitutive model for the triaxial behavior of concrete", presented at Istituto Sperimentale Modelli e Strutture (ISMES), Bergamo, Italy, May, 17–19, 1974.
- [36] El-Mogy, M. "Behaviour of continuous concrete beams reinforced with FRP bars", PhD Thesis, University of Manitoba, 2011.
- [37] Kachlakev, D. I., Miller, T. H., Yim, S., Chansawat, K., Potisuk, T. "Finite element modeling of reinforced concrete structures strengthened with FRP laminates", Department of Transportation, Oregon, USA, Rep. FHWA-OR-RD-01-XX, 2001.
- [38] Wolanski, A. J. "Flexural behavior of reinforced and prestressed concrete beams using finite element analysis", MSc Thesis, Marquette University, 2004.
- [39] Gibbons, N., Fanning, P. J. "Progressive cracking of masonry arch bridges", *Proceedings of the Institution of Civil Engineers: Bridge Engineering*, 169(2), pp. 93–112, 2016.  
<https://doi.org/10.1680/jbren.15.00009>

- [40] Pelà, L., Aprile, A., Benedetti, A. "Comparison of seismic assessment procedures for masonry arch bridges", *Construction and Building Materials*, 38, pp. 381–394, 2013.  
<https://doi.org/10.1016/j.conbuildmat.2012.08.046>
- [41] Altunişik, A. C., Kalkan, E., Okur, A. Y., Karahasan, O. Ş., Ozgan, K. "Finite-element model updating and dynamic responses of reconstructed historical timber bridges using ambient vibration test results", *Journal of Performance of Constructed Facilities*, 34(1), 4019085, 2020.  
[https://doi.org/10.1061/\(ASCE\)CF.1943-5509.0001344](https://doi.org/10.1061/(ASCE)CF.1943-5509.0001344)
- [42] Forgács, T., Rendes, S., Ádány, S., Sarhosis, V. "Mechanical role of spandrel walls on the capacity of masonry arch bridges", In: 9th International Conference on Arch Bridges (ARCH 2019), Porto, Portugal, 2019, pp. 221–229. ISBN 9783030292263.  
[https://doi.org/10.1007/978-3-030-29227-0\\_21](https://doi.org/10.1007/978-3-030-29227-0_21)
- [43] Forgács, T., Sarhosis, V., Ádány, S. "Shakedown and dynamic behaviour of masonry arch railway bridges", *Engineering Structures*, 34, 111474, 2021.  
<https://doi.org/10.1016/j.engstruct.2020.111474>
- [44] Geraschenko, V. S., Grishin, A. S., Gartung, N. I. "Approaches for the calculation of rayleigh damping coefficients for a time–history analysis", In: Syngellakis, S., Schleyer, G. (eds.), *Structures Under Shock and Impact XV*, 180, WIT Press, 2018, pp. 227–237. ISBN 978-1-78466-265-3  
<https://doi.org/10.2495/SUSI180201>
- [45] Ministry of Transport and Infrastructure "Bridge Earthquake Code of Turkey, Principles for the design of road and rail bridges and viaducts under earthquake effect", Ankara, Turkey, 2020. (in Turkish)
- [46] General Directorate for Foundations "Building Earthquake Code of Turkey BECT-2018", Ankara, Turkey, 2018. (in Turkish)
- [47] Seismosoft Ltd. "SeismoArtif (2021)" [software] Available at: <https://seismosoft.com/product/seismoartif/> [Accessed: 15 April 2022]
- [48] Ministry of Transportation "Earthquake Technical Regulations Relating to Coastal, Harbor, Railway and Airport Constructions", Ankara, Turkey, 2007. (in Turkish)
- [49] Saragoni, R. G., Hart, G. C. "Simulation of artificial earthquakes", *Earthquake Engineering & Structural Dynamics*, 2(3), pp. 249–267, 1973.  
<https://doi.org/10.1002/eqe.4290020305>